Journal of Biomedical Optics 9(4), 804–819 (July/August 2004)

Nonintrusive, noncontacting frequency-domain photothermal radiometry and luminescence depth profilometry of carious and artificial subsurface lesions in human teeth

Raymond J. Jeon
Andreas Mandelis
Victor Sanchez
Center for Advanced Diffusion-Wave Technologies
Department of Mechanical and Industrial Engineering
University of Toronto
5 King's College Road
Toronto, Ontario
M5S 3G8, Canada
E-mail: mandelis@mie.utoronto.ca

Stephen H. Abrams
Four Cell Consulting
748 Briar Hill Avenue
Toronto, Ontario
M6B 1L3, Canada

Abstract. Nonintrusive, noncontacting frequency-domain photothermal radiometry (FD-PTR or PTR) and frequency-domain luminescence (FD-LUM or LUM) have been used with 659-nm and 830-nm laser sources to detect artificial and natural subsurface defects in human teeth. The major findings of this study are (1) PTR is sensitive to very deep (>5 mm) defects at low modulation frequencies (5 Hz). Both PTR and LUM amplitudes exhibit a peak at tooth thicknesses of ca. 1.4 to 2.7 mm. Furthermore, the LUM amplitude exhibits a small trough at ca. 2.5 to 3.5 mm. (2) PTR is sensitive to various defects such as a deep carious lesion, a demineralized area, an edge, a crack, and a surface stain, while LUM exhibits low sensitivity and spatial resolution. (3) PTR frequency scans over the surface of a fissure into demineralized enamel and dentin show higher amplitude than those for healthy teeth, as well as a pronounced curvature in both the amplitude and phase signal channels. These can be excellent markers for the diagnosis of subsurface carious lesions. (4) PTR amplitude frequency scans over the surface of enamels of variable thickness exhibit strong thickness dependence, thus establishing depth profilometric sensitivity to subsurface interfaces such as the dentin/enamel junction.
[DOI: 10.1117/1.1755234]

Keywords: dental photothermal radiometry, modulated luminescence, depth profilometry, subsurface imaging, dental caries.

Paper 03058 received Apr. 30, 2003; revised manuscript received Nov. 4, 2003; accepted for publication Nov. 24, 2003.

1 Introduction

In the past few decades, with the widespread use of fluoride, the prevalence of caries, especially smooth surface caries, has been considerably reduced.[1,2] For example, it was reported that a 50% reduction of smooth surface caries had been documented for 17-year-olds over the period 1971 to 1985.[3] However, a greater reduction in smooth surface caries has resulted in an increase in the proportion of primary small caries in pits and fissures (biting surface) of teeth.[1] The fact that small lesions have the potential to remineralize if preventive measures are applied in time has prompted efforts to develop and improve diagnostic methods to enable detection of early lesions that cannot be disclosed by visual inspection.[4] Therefore, the development of (preferably noncontacting) techniques and instruments that can detect early demineralization or tiny lesions on or beneath the enamel surface has been an active area of research for the past decade. The use of lasers for dental diagnostics is considered to be promising in this area, mainly through the phenomenon of laser-induced fluorescence of the enamel.

Eggertsson et al.[5] evaluated the uses of laser fluorescence (LF) and dye-enhanced laser fluorescence (DELF), compared them with a visual examination, and found the DELF was better in sensitivity, but the DELF and visual examination were better than LF in specificity. As an effort to quantify fluorescence based on the quantitative light-induced fluorescence (QLF) technique, various devices such as a ring illuminator, a beamsplitter, and a clinical caries camera were compared by Lagerweij et al.[6] Another study by Verdonschot et al.[7] comparing fiber-optic transillumination (FOTI), electrical resistance measurements (ERM), radiography, and visual inspection, showed that those new techniques were not much better than visual inspection. However, they pointed out that the quantitative caries detection methods (QLF, ERM, and FOTI) were preferable for monitoring the progression of disease. The presence of caries could be observed by inexpensive visual inspection, but then caries preventive strategies would be initiated too late because the lesions had grown large and at times involved the dentin. Therefore, for early detection of small initial subsurface lesions, the development of new nonintrusive, noncontacting techniques is necessary.

Address all correspondence to Prof. Andreas Mandelis, Univ. of Toronto, Ontario, M5S 3G8, Canada. E-mail: mandelis@mie.utoronto.ca

1083-3668/2004/$15.00 © 2004 SPIE

The DIAGNOdent[8,9] is a device for detecting occlusal caries based on laser fluorescence which can distinguish carious and healthy teeth using dc laser excitation. According to the inventors, laser-intensity modulation can also be utilized to eliminate background noise[9] in the collection of luminescence from a tooth. The device is based upon the fluorescence caused by porphyrins present in carious tissue and not the amount of enamel demineralization.[10] Porphyrin fluorescence may also lead to false positives since these are found in stained but healthy fissures. A number of studies were performed to assess the feasibility of using this device,[11–13] and it has been evaluated as having the potential to improve caries assessment in many ways. Specifically, its high reproducibility was claimed to be an outstanding benefit of this device. Nevertheless, a validity study involving the DIAGNOdent concluded that using dc luminescence was not statistically significantly different from visual inspection.[10] Furthermore, it was concluded that the DIAGNOdent was suitable for detecting small superficial lesions, rather than deep dentinal lesions.[10]

Generally, it appears that fluorescence induced through continuous (dc) irradiation of a tooth suffers from low signal level.[14] To enhance the intensity of the fluorescence signal, sodium fluorescein was used to dye the carious part, but as previously stated, this DELF technique did not show significant enhancement over laser fluorescence or visual examination.[5] Recently, time-resolved (pulsed-laser-induced) infrared photothermal radiometry (PPTR)[15,16] was used to determine the absorption coefficients of dental enamel at 9.6, 10.3, and 10.6 μm, the results of which are potentially important in the application of CO_2 lasers for the ablation of hard dental tissue.[17] High-power pulsed lasers, such as erbium (Er:YSGG), erbium yttrium aluminum garnet (Er:YAG) or CO_2, have also been used to measure surface and subsurface temperatures during the irradiation of dental enamel.[15,16] The first attempt to apply the depth profilometric capability of frequency-domain PTR toward the inspection of dental defects was reported by Mandelis et al.[18] and Nicolaides et al.,[19] and was recently reviewed by Mandelis.[20] This is a novel dynamic (i.e., nonstatic) dental depth profilometric inspection technique that can provide simultaneous measurements of intensity-modulated laser-induced frequency-domain infrared photothermal radiometric (FD-PTR) and luminescence (FD-LUM) signals from defects in teeth.[18,19]

FD-PTR is a growing technology and has been applied, among other areas, to the nondestructive evaluation (NDE) of subsurface features in opaque materials.[21] It has also shown promise in the study of excited-state dynamics in optically active solid-state (laser) materials.[22] The technique is based on the modulated thermal infrared (black-body or Planck radiation) response of a medium resulting from radiation absorption and nonradiative energy conversion followed by a temperature rise. The generated signals carry subsurface information in the form of a temperature depth integral. Thus, PTR has the ability to penetrate, and yield information about, an opaque medium well beyond the range of optical imaging. Specifically, the frequency dependence of the penetration depth of thermal waves makes it possible to do depth profiling of materials.[23]

In dental applications, an early attempt to use the well-established technique of phase-sensitive modulated infrared thermography to obtain thermal infrared dental images with a camera showed good promise in resolving various thermal structures of a ground section of a resin-embedded extracted human tooth.[24] The thermographic magnitude and phase images exhibited better contrast at the low frequency of 0.06 Hz than 0.23 Hz imaging. This type of phase-sensitive thermographic imaging requires low frequency for best contrast, which is too slow for dental practice; it also requires significant sample preparation (slicing, grinding, and encasing in a resin matrix), which cannot be implemented clinically *in vivo*. Furthermore, it is often desirable in dental practice to obtain detailed local information on potential lesions, and inside pits and fissures with high spatial resolution, such as that achieved with a focused laser source. To meet these objectives, recently, a combination of FD-PTR and FD-LUM was used as a fast dental diagnostic tool to quantify sound enamel or dentin as well as subsurface cracks in human teeth.[19]

Under 488-nm laser excitation and frequencies in the range of 10 Hz to 10 kHz, it was found that PTR images are complementary to LUM images as a direct result of the complementary nature of nonradiative and radiative deexcitation processes, which are responsible for the PTR and LUM signal generation, respectively, at that wavelength. It was also concluded qualitatively that radiometric images are depth profilometric (meaning they yield depth-dependent information as a function of the laser beam modulation frequency), but no definitive conclusions regarding the depth profilometric character of LUM were reached.

Finally, LUM frequency responses from enamel and hydroxyapatite were found to exhibit two relaxation lifetimes, the longer of which ($\sim$ milliseconds) is common to all teeth (including canine) and is not sensitive to the defect state or the overall quality of the enamel. A degree of sensitivity to enamel quality was established for the shorter ($\sim$ microseconds) lifetime. Furthermore, our group has introduced theoretical models of FD-PTR and FD-LUM that can yield quantitative values of optical and fluorophore parameters of sound enamel.[25] Unique sets of the optical parameters (μ_α, optical absorption coefficient; μ_S, scattering coefficient; $\bar{\mu}_{IR}$, spectrally averaged infrared emission coefficient) of enamel and its fluorophore relaxation time constants (τ_1, τ_2) were obtained using the theory with a three-dimensional photothermal multiparameter fit formulation and inputs from LUM and PTR data.[25]

In this study, three sets of experiments were performed to evaluate the depth profilometric imaging capabilities of FD-PTR and FD-LUM in monitoring carious and artificial subsurface lesions in human teeth. The first set involves sectioning and preparing several teeth. The goal was to determine the subsurface penetration depth and spatial resolution of PTR and LUM signals to artificial lesions of high contrast. In the second set, extracted human teeth with various natural types of near-surface and deep subsurface lesions (a demineralized carious fissure, a deep subsurface carious lesion in dentin, an enamel crack, a surface stain, an extended cavity on the opposite side of a tooth) were examined. Finally, the PTR and LUM responses to variations in enamel thickness were examined to assess the overall penetration depth of these probes. As a result of these studies of the behavior of PTR and LUM signals in the presence of some common natural and artificial defects and lesions, the potential for the frequency-domain

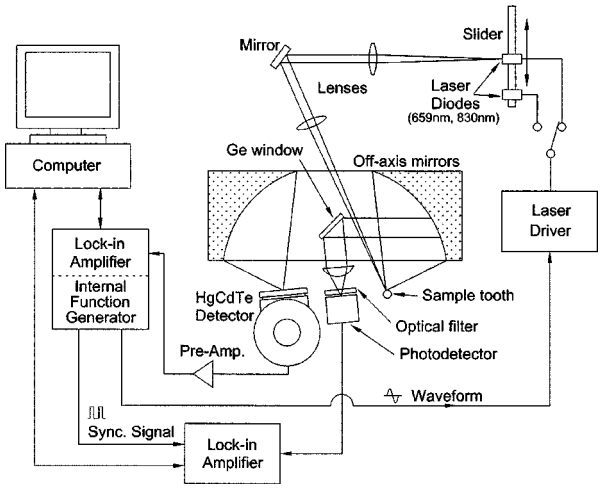

Fig. 1 Schematic diagram of experimental setup for combined PTR and LUM monitoring.

PTR and LUM signals as dental depth profilometric diagnostic methodologies has been assessed.

2 Materials and Methods

2.1 *Sample Preparation*

Several extracted human teeth were separately stored in vials in saline solution before the experiments to avoid dehydration and contamination. Each sample tooth in the study was removed from the vial, rinsed thoroughly with clean water for more than 20 s, and then dried with pressurized air. Then the tooth was placed on the sample stage and the laser was turned on and focused on the sample tooth by adjusting a three-axis micrometer stage. This process usually takes about 20 min before starting measurements, during which time the tooth is dehydrated properly. This protocol was adhered to because dehydration of a tooth sample affects its optical qualities, such as light scattering and fluorescence, as well as thermal properties. Al-Khateeb et al.[17] showed that the fluorescence radiance of sound enamel and enamel lesions decreased from that of wet enamel for about 2 to 20 min, depending on the sample, before becoming steady. Therefore, 20 min of preparation time appears to be necessary to avoid the effect of hydration. Moreover, since the surface temperature of the sample could be slightly decreased during washing with water and drying with compressed air, there is a need to wait until the sample thermalizes at the ambient temperature.

2.2 *Experimental Setup*

Figure 1 shows the experimental setup for combined PTR and LUM probing. Two different semiconductor lasers were used. Their wavelengths and maximum powers were 659 nm and 30 mW (Mitsubishi ML1016R-01) and 830 nm and 100 mW (Sanyo DL-7032-001), respectively. These lasers were mounted on a stage with a sliding base so that they could be brought into the optical circuit by simply sliding the base. A common diode laser driver (Coherent 6060) triggered by the built-in function generator of the lock-in amplifier (Stanford Research SR830) modulated the laser current harmonically. The laser beam was focused on the sample with a high-performance lens (Gradium GPX085) to a spot size of approximately 55 μm for the 659-nm laser and 326 μm for the 830-nm laser. The modulated infrared PTR signal from the tooth was collected and focused by two off-axis paraboloidal mirrors onto a mercury cadmium telluride (HgCdTe or MCT) detector (EG & G Judson J15D12-M204-S050U). Before being sent to the lock-in amplifier, the PTR signal was amplified by a preamplifier (EG & G Judson PA-300). For the simultaneous measurement of PTR and LUM signals, a germanium window was placed between the paraboloidal mirrors. This was utilized so that wavelengths up to 1.85 μm (Ge band gap) would be reflected and absorbed, while infrared radiation with longer wavelengths would be transmitted. The reflected luminescence was focused onto a photodetector of spectral bandwidth 300 nm to 1.1 μm (Newport 818-BB-20). A cut-on colored glass filter (cut-on wavelength, 715 nm, Oriel 51345) was placed in front of the photodetector to block laser light reflected or scattered by the tooth. For modulated luminescence monitoring, another lock-in amplifier (EG & G model 5210) was used. Both lock-in amplifiers were connected to, and controlled by, the computer via RS-232 ports.

2.3 *Experimental Procedure*

Two kinds of experiments were performed. One was a frequency scan to examine the frequency dependence of the PTR and LUM signals from 1 Hz to 1 kHz. The frequency range was divided into 40 equal intervals on a logarithmic scale by the data acquisition computer program, and the frequency was automatically increased after each measurement. There was a 15-s time delay between the measurements at each frequency, which was necessary for stabilizing the signals when the frequency was changed. Each point was measured five times and the data were averaged. The total measurement time for one frequency scan was about 40 min. The other type of experiment measured the PTR and the LUM signals along a spatial coordinate on the tooth surface at a fixed frequency. Because each tooth had an irregular surface, the focal length of the laser beam had to be adjusted accordingly at each measurement position. In this spatial scan, 2 to 3 min per position were needed to adjust the focal point and do the measurement. As with the frequency scans, a measurement at a new position was performed 15 s after moving the laser beam to that position.

3 Results and Discussion

The salient features of PTR and LUM signals from dental tissues can be summarized as follows. Since enamel (and generally the whole tooth) is a turbid medium, optical penetration is controlled by the optical extinction coefficient, μ_{ex} (a combination of optical absorption and scattering coefficients) at a given excitation wavelength.[25] For an estimate of the extinction coefficient under irradiation with the two wavelengths used in this study, Fried et al.[26] reported a scattering coefficient, μ_s, for enamel of between $15 \pm 5\ \mathrm{cm}^{-1}$ (at 1053 nm) and $60\ \mathrm{cm}^{-1}$ (at 632 nm), while the absorption coefficient, μ_a, was less than $1\ \mathrm{cm}^{-1}$. For dentin, the scattering coefficient was between $260 \pm 78\ \mathrm{cm}^{-1}$ (at 1053 nm) and $280 \pm 84\ \mathrm{cm}^{-1}$ (at 632 nm), while the absorption coefficient was 3 to $4\ \mathrm{cm}^{-1}$.

Photothermal techniques such as PTR respond only to thermal occlusion following optical absorption and thus are in principle less affected by scattered light, which does not produce heat because most scattered photons simply leave the field of view of the IR detector. Therefore, PTR is capable of ''seeing through'' the optically (but less so thermally) interfering turbid optical field, and the laser source can deposit energy as deep as the optical absorption depth, μ_a^{-1}, which, in teeth, lies between 0.3 and 1 cm in the foregoing (and our) range of wavelengths. Of course, scattering does tend to diminish the optical intensity reaching those deep regions.[25] Furthermore, absorption and scattering of thermal infrared photons emitted from the probed medium tend to compromise the observable signal from deep regions.

PTR detection in turbid and other nonopaque media is controlled by a combination of harmonic thermal conduction signals from near-subsurface regions and is characterized by a thermal diffusion length associated with the particular modulation frequency and thermal infrared (Planck) emissions from deeper regions. In the conductive mode, the depth sensitivity of the PTR signal is theoretically limited to up to one or two thermal diffusion lengths, $\mu(f)$, where $\mu(f)=(\alpha/\pi f)^{1/2}$, α is the material thermal diffusivity (cm^2/s) and f is the laser modulation frequency (Hz). μ is approximately 386, 173, 71, and 12 μm at 1 Hz, 5 Hz, 30 Hz, and 1 kHz, respectively; the thermal diffusivity of enamel is 4.69×10^{-3} cm^2/s.[27]

Based on the foregoing description, PTR amplitudes and phases both carry subsurface information in a conductive, diffusively spatially weighed depth-integral form from near-surface absorptions that are limited by the thermal diffusion length (shallow features) as well as the superposed thermal infrared radiative heat transfer, synchronously modulated at the laser excitation frequency, from depths limited by the optical extinction length. Enhanced radiative photon emission information from deep profiles originates in optically absorbing and heat-releasing subsurface features like a carious lesion. PTR phase lags are mostly sensitive to conductive thermal-wave generation because thermal-radiation infrared photons can reach the detector without time delay (speed of light) at frequencies used for dental diagnostics provided they are not substantially reabsorbed by the surrounding medium (the case with dental PTR).

Because the thermal-wave phase is the ratio of quadrature and in-phase lock-in signals, it is in principle independent of both surface optical reflectance and infrared emissivity contributions to the PTR signal, unlike the PTR amplitude. Therefore, the PTR phase represents a true thermal-wave signature in the conductive regime, but amplitude is more sensitive to prompt radiative emissions, which carry little phase information. Depth profilometry is obtained from subsurface contributions to both thermal mechanisms; however, radiative and conductive weights are different in the two channels (see the case studies below).

On the other hand, LUM signals, like X-rays, are not diffusive. Thus different subsurface regions contribute equally to the signal in the form of a line integral, as long as optical absorption can be induced through the interfering scattering region. Therefore LUM is largely nondepth profilometric. Because LUM signals are purely the result of optical-to-optical energy conversion and red-shifted photon emission, there is no phase delay information other than that associated with optical phenomena such as chromophore deexcitation time constants.[19] Nevertheless, as with any light wave, phase is influenced by spatial optical interference, reflection, and scattering.

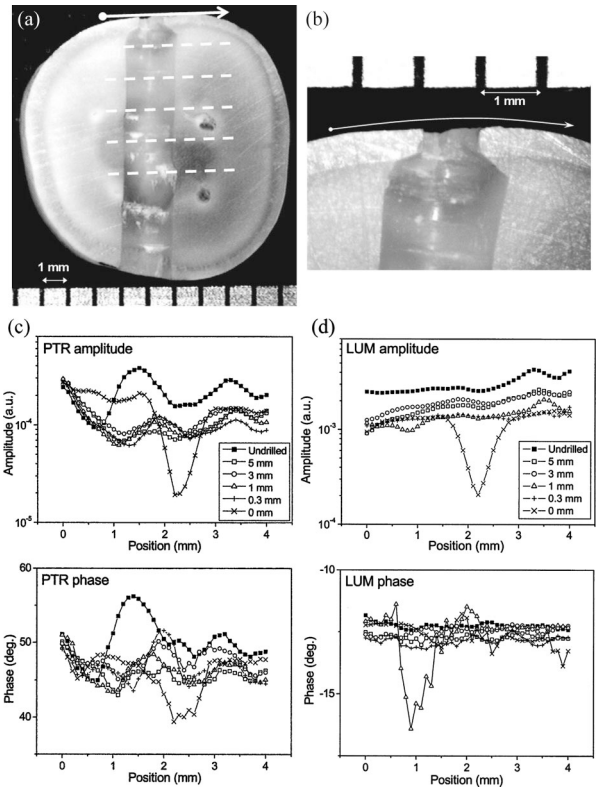

Fig. 2 Cross-sectional photographs and experimental results of the sample tooth, case I-A. (a) Transverse cross-section at the scan line along the center of a drilled hole. Magnified view of the whole cross-section (the white arrow is the scanning line and the white dotted lines show the depths from the scanned surface at 1-mm intervals). (b) Magnified view of a laser scan across the drilled hole region (white arrow). (c) PTR amplitude and phase signals across the scan line at various depths of the tip of the drilled hole at 5 Hz with the 659-nm laser. The inset indicates distances from the scanned surface. (d) LUM amplitude and phase signals corresponding to Fig. 2(c) at 5 Hz with the 659-nm laser.

3.1 *Case I. Detection of Artificial Subsurface Holes and Variations in Tooth Thickness*

3.1.1 *Drilled subsurface holes at variable depths from tooth surface*

In order to examine whether an artificially drilled hole can influence either the PTR or the LUM signals, or both, spatial scans on a side surface of a mandibular molar were performed with the 659-nm laser at 5 Hz after gradual drilling of a hole from the opposite side (case I-A). The hole was drilled in the middle third of the tooth just at the base of two very deep fissures. Figure 2(a) shows a cross-sectional view of the drilled hole in the sample at the end of the experiments. The depth of each hole from the scanned surface at each measured interval is also marked. The two holes to the right of the grooves are the bottoms of the fissures which were visible on the top surface. A magnified view of the scan line is shown in

Fig. 2(b). This cross-section illustrates the changing mineral content as the dentin approaches the pulp chamber. Close to the pulp chamber, there is less mineralized tissue and there are more tubules containing tissue fluids and odontoblast processes.

As shown in Fig. 2(c), the PTR amplitude and phase changed greatly when the first hole was made. The distance from the scanned surface [along the arrow on the top of the picture in Fig. 2(b)] to the bottom of the drilled hole after the first drilling was approximately 5 mm. The large change in the PTR signal scan from the intact level is indicative of the depth-integral contributions to the PTR signal along the entire thickness (or substantial portion thereof) of the tooth. It seems to be caused by drilling out a large dark area (dentin very close to the pulp chamber) in the middle of the tooth, with two district lobes corresponding to the two signal peaks. Vestiges of the area are still visible in Fig. 2(a). A major part of this deep, slightly mineralized dentin was removed by the first drilling. It is hypothesized that the diminished sensitivity to subsurface features after the first drilling occurs because the major part of the dark region, which was not as mineralized as the surrounding dentin, had already been removed by the initial drilling. That was the source of strong light absorption and thermal IR emissions. As the hole was drilled farther, there were no comparably large changes in the PTR amplitude.

With regard to the deep subsurface features of Fig. 2(c), it is the thermal infrared radiation emission mode of PTR that can only be responsible for the observed depth profilometry of the subsurface structure. The LUM amplitude and phase in Fig. 2(d) also show substantial differences after the first drilling that are consistent with the removal of a luminescent source, albeit with less contrast than the PTR signals. LUM detection is also characterized by radiative emissions from the optically excited region within the luminescence bandwidth of the tooth ($\sim$700 to 800 nm).[8,9] At much smaller thicknesses of enamel ($<500\ \mu$m), PTR sensitivity is once again reestablished owing to conductive heat transfer within approximately one thermal diffusion length. No such mechanism is, of course, available to the LUM channel.

Optical interference within very thin enamel regions (<1 mm) of variable thickness is possibly the origin of the LUM structure shown in Fig. 2(d). The thin enamel surface was broken away when the drill tip reached the surface (thickness$=0$ mm), and the PTR amplitude around the gaping hole increased because of the very thin enamel layer and edge effects.[28] With these results, it was concluded that PTR and LUM are able to detect subsurface defects or changes in mineralization with sharp boundaries at depths greater than 5 mm, with PTR exhibiting superior sensitivity and contrast for both the presence of, and changes in, the sharp boundaries, as well as changes in mineral content (dark regions) of the tooth.

3.1.2 *Subsurface grooves oriented with respect to proximal tooth surface*

To complement the foregoing results, artificial wide grooves were made normal to the transversely sectioned surface plane of a mandibular molar (case I-B). Figure 3(a) shows top-down photographs of the prepared tooth. Figure 3(a) 1 is that of the cross-section with several predrilled holes and an upper groove, including holes labeled H_0 and H_3 used in this study. Figure 3(a) 2 shows a new wide groove joining holes H_0 and H_3. The groove is nearly parallel to the flat exterior side (proximal) surface of the tooth at a distance of about 3 mm. The holes labeled H_1 and H_2 were formed by the lateral motion of the drill in creating the groove as the drill encountered the pulp chamber, which is shown in cross-section in Fig. 3(b). Figure 3(a) 3 shows the same groove further widened to produce a slanted front edge with respect to the scanned proximal surface. The approximately 1-mm distance from the top surface and the lateral extent of the laser scans is indicated in Fig. 3(b) with an arrow. This figure shows a side view of the (eventually cut-away) cross-section A-A in Figs. 3(a) 3. It also shows a view of the back surface of the front groove of Fig. 3(a) 3. It reveals the pulp chamber situated in the middle of the tooth and just below the bottom of the groove in Fig. 3(a).

Spatial line scans were performed on this sample with both lasers at two different frequencies, 5 and 30 Hz. As a result, some interesting features were found. The initial PTR signals of Figs. 3(c) and 3(d) corresponding to Fig. 3(a) 1 show peaks at the positions of the preexisting holes H_0 and H_3. The spatial resolution of the PTR signal, both amplitude and phase, improves at the higher frequency of 30 Hz under 659-nm detection [Fig. 3(d)]. This is expected from the shortened thermal wavelength, which further localizes the interaction of the photothermal field with the subsurface defects. The deeper-penetrating 830-nm radiation generates equal or better PTR amplitude resolution for the H_0 and H_3 holes of Fig. 3(a) 1. This is seen in Figs. 3(e) and 3(f), with decreased thermal confinement at 30 Hz compared with Fig. 3(d), which is due to the deeper penetration of the 830-nm light. For the same reason the amplitude of the 830-nm PTR signal is smaller.

These features are expected from the more deeply penetrating 830-nm radiation, where direct infrared blackbody emissions within the optical extinction (absorption and scattering) length are more likely to control PTR depth resolution instead of diffusive heat transfer within the modulation-frequency-dependent thermal diffusion length. It is also noted that 830-nm PTR phases are less sensitive to the presence of the two normal holes H_0 and H_3 [Figs. 3(e) and 3(f)], which is most likely a feature of the radiative emission domination of the deeper penetrating light at the expense of the conductive component, so that no significant phase information is expected or, indeed, observed. No LUM data were possible under 830-nm excitation, since luminescence emission requires irradiation with higher-energy photons than the peaks of luminescence at ca. 636, 673, and 700 nm.[8] LUM data of the initial scan of Fig. 3(a) 1 under 659-nm laser excitation exhibit much compromised resolution of the normal holes H_0 and H_3 [Figs. 3(g) and 3(h)], compared with the PTR scans.

After the full groove shown in Fig. 3(a) 2 was drilled out, the PTR scans exhibited an overall decrease in amplitude [Figs. 3(c) and 3(e) and 3(d) and 3(f)]. The "line-of-sight" overlap of the predrilled rightmost normal hole H_3 in Fig. 3(a) 1 and the hole H_2 in Fig. 3(a) 2 is unresolvable in the PTR amplitude signals of Figs. 3(c) and 3(d). It is interesting, however, to note that the line scans of the 830-nm PTR amplitude and phase in Fig. 3(e) at 5 Hz are able to resolve the presence of the holes H_1 and H_2 at approximate positions of 1.5 and 2.5 mm, respectively. The presence of these holes is also seen in

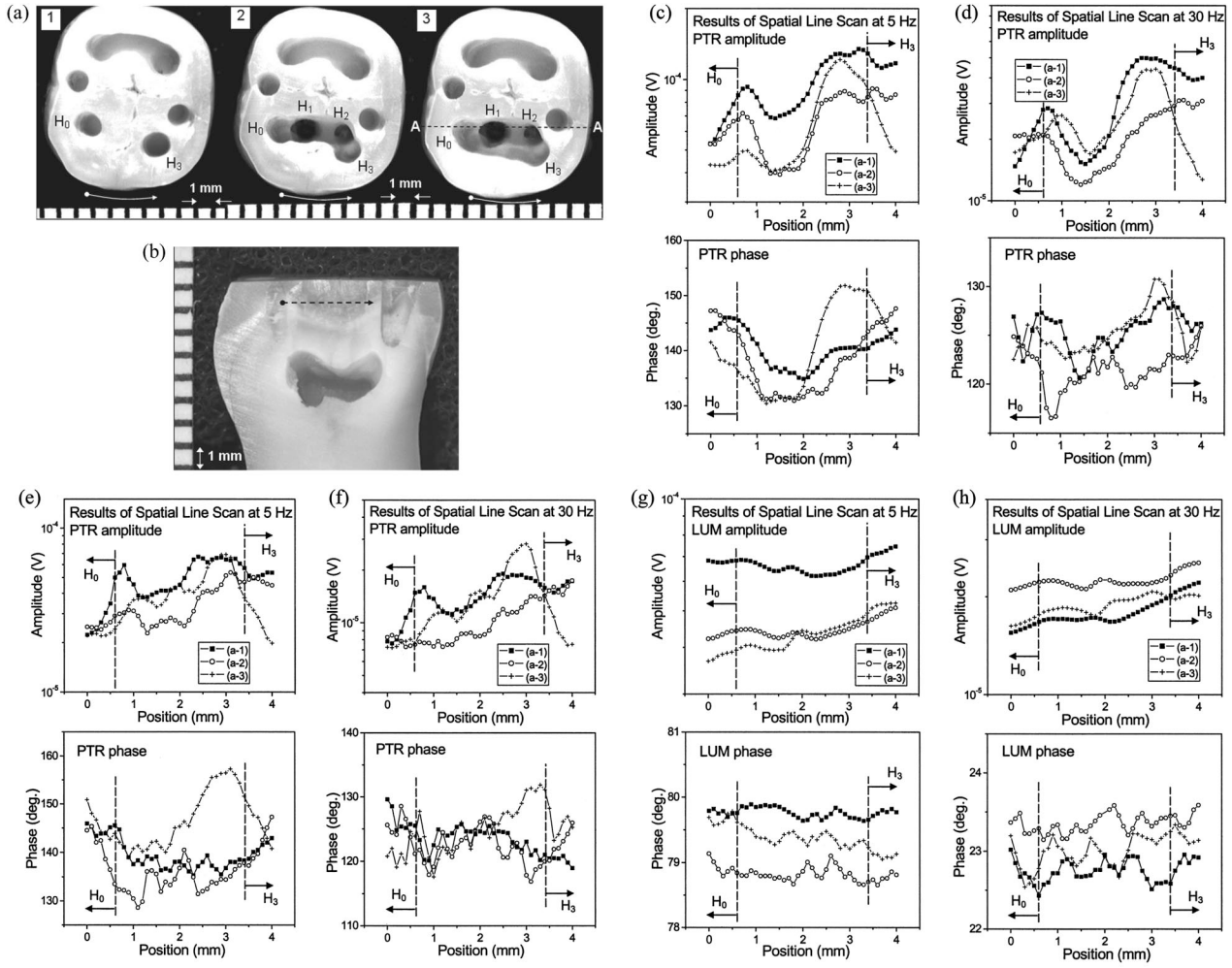

Fig. 3 Cross-sectional photographs and experimental results of the sample tooth, case I-B. (a) Top-down photographs of the cross-sectioned and prepared tooth, with several holes and scan lines marked (white arrows at the bottom). 1, initial configuration of the sample; 2, after preparing a groove horizontal to the biting surface of the tooth; 3, after widening the groove into a wider slanted hole. (b) Side view of cross-section A-A in (a3) showing a deeper hole at the location of the pulp cavity; the arrow indicates the scan coordinate. (c) PTR amplitude and phase signals across the scan line (arrow) for configuration (a) 1 to (a) 3 at 5 Hz with the 659-nm laser. (d) Similar to (c) at 30 Hz. (e) Similar to (c) with the 830-nm laser. (f) Similar to (e) at 30 Hz. (g) LUM amplitude and phase signals across the scan line at 5 Hz with the 659-nm laser. (h) Similar to (g) at 30 Hz.

the 30-Hz scan of Fig. 3(f) with improved resolution over the 5-Hz scan.

The PTR phase of the 659-nm scan at 30 Hz [Fig. 3(d)] also exhibits excellent sensitivity to the larger hole, H_1, but the confluence of features H_2 and H_3 close to the right edge of the scan is such that no specific trend appears in the phase there. The LUM scans of Figs. 3(g) and 3(h) do not exhibit as good a resolution of the H_1 and H_2 features as their PTR counterparts; nevertheless, the LUM amplitude at 5 Hz decreases and at 30 Hz increases with respect to the initial scans. These opposite trends can be explained when the transmission of optical excitation power across the front edge of the groove and the dental luminescence generation dynamics are taken into account. Direct optical power transmitted past the groove edge does not contribute to backscattered luminescence. The remaining optical excitation field that produces the LUM (and PTR) signals is confined between the outer surface of the tooth and the groove edge, thus shifting the diffuse photon-density-wave centroid of the optical excitation density, the thermal-wave, and the luminescence diffuse photon-density-wave centroids closer to the surface, resulting in a decreased LUM phase lag at 5 Hz [Fig. 3(g)], as well as decreased PTR phase lags at both frequencies [Figs. 3(c) and 3(d)].[29]

Unlike the 5-Hz case, however, the LUM signal at 30 Hz is subject to strong hydroxyapatite deexcitation lifetime relaxation effects,[19] which dominate under spatial confinement conditions (presence of a groove) and increase the phase lag as observed in Fig. 3(h). The expected concomitant decrease in LUM amplitude[19] is compensated by optical or luminescence confinement at the back enamel/air interface, thus resulting instead in a net increase of the amplitude in Fig. 3(h). This is further corroborated by studies of signal dependence on enamel thickness (see case III).

Finally, after the widened, slanted groove of Fig. 3(a) 3 was drilled out, the PTR amplitudes increased compared with those obtained from Fig. 3(a) 2, and the rightmost peak, centered at approximately 3 mm owing to the widened hole H_3, strongly reappeared. The PTR amplitude and phase ratios of

the (H_2, H_3) to (H_0, H_1) peaks [Figs. 3(c)–3(f)], increased significantly after the slanted groove was drilled out, owing to the closer proximity of the edges of H_3 to the scanned proximal surface and the general slant of the outer edge in Fig. 3(a) 3 toward the surface.

The closer proximity of the (H_2, H_3) region to the surface further caused the appearance of the 3-mm phase peaks in Figs. 3(c) to 3(f). Regarding the peak width of the (H_2, H_3) feature, a narrowing appears at 30 Hz compared with 5 Hz at 659 nm, as expected and previously discussed. An overall narrow peak similar to the 30-Hz peak of Fig. 3(d) appears under 830-nm scanning, at 5 Hz and 30 Hz alike. In addition, the structure from the region between holes H_1 and H_2 (1 to 2.5 mm), evident in both PTR amplitude and phase signals before the widening of the groove [Figs. 3(e) and 3(f)], remains under the 830-nm probe after the widening of the groove. The structure is not present in the 659-nm scans, except mildly so in the 30-Hz phase [Fig. 3(d)]. These results are consistent with greater infrared radiative emissive control of the PTR signal under 830-nm irradiation and greater thermal-wave control of the 659-nm signals, respectively. The LUM resolution, however, remained quite poor, as shown in Figs. 3(g) and 3(h), with only a trace of the rightmost peak centered at ca. 3 mm and a relatively broad leftmost peak trace centered at ca. 1 mm. Figure 3(g) shows that the 5-Hz LUM phase is sensitive to the H_0-H_3 hole structure, but there is no evidence of the depth-related weighting factor that generates the strong (H_2, H_3) PTR signal phase in Figs. 3(c) and 3(e).

Further narrowing of the solid enamel-dentin strip with the groove widening of Fig. 3(a) 3, brings about greater thermal-wave confinement within the strip than in Fig. 3(a) 2, which increased the PTR amplitude under excitation with both wavelengths. Nevertheless, the large phase peaks (lags) in Figs. 3(c) and 3(f) around 3 mm [at the (H_2, H_3) hole position] are indicative of considerable heat transport across the back tooth/air boundary of the slanted groove. This component of the thermal wave can extend quite far inside the groove by virtue of the thermal diffusivity of air, which is significantly higher (0.19 cm^2/s) than that of teeth (4.69×10^{-3} cm^2/s),[27] thus dragging the thermal-wave centroid much deeper into the bulk of the tooth and making the deep subsurface (H_2, H_3) hole structure clearly visible photothermally, despite the diffuse nature of the exciting optical field.

Much milder effects are shown in the LUM signals with the widening and slanting of the groove. The amplitude signal at 30 Hz exhibits a general decrease with groove widening on going from the confiuguration of Fig. 3(a) 2 to Fig. 3(a) 3, owing to enhanced loss of the optical source energy across the front-groove edge [Fig. 3(h)], with the expected concomitant phase lag decrease that is due to the confinement of the LUM signal generating a diffuse photon-density-wave centroid within the tooth region closer to the scanned proximal surface. Under 5-Hz excitation, the effect of luminescence loss into the widened groove amounts to a small decrease in the LUM amplitude between 0 and 2 mm, where the widening is most pronounced, with a concomitant increase in the phase lag that is consistent with the enhanced contribution of the deep subsurface signal source (laser power transmitted past the front edge of the groove). This is further consistent with the greater lag of the PTR phase at 5 Hz and 830-nm excitation [Fig. 3(e)], where optical transmission occurs deeper into the groove.

In summary, the results of Fig. 3 show that PTR line imaging has depth profilometric capabilities, monitoring artificial defects at least up to 3 mm below the surface. LUM line imaging is largely nonprofilometric, but nevertheless exhibits some depth resolution features that are primarily associated with optical source and luminescence confinement between interfaces across sharp tooth/air boundaries. Overall, LUM appears to exhibit much lower resolution and contrast for localized, artificially made, subsurface defects in teeth than PTR does.

3.1.3 *Thickness variations in healthy and carious teeth*

One intact tooth and another tooth with a deep carious lesion on the opposite side were frequency scanned from 1 Hz to 1 kHz with the two lasers (case I-B). After each scan, a thin slice of the opposite side was ground off so that the thickness varied from 10.2 to 0.6 mm [intact tooth; Figs. 4(a) and 4(b)] and from 8 to 1.7 mm [carious tooth; Figs. 5(a) and 5(b)]. Figure 4(b) and Fig. 5(b) show top-down views of intermediate thickness stages of these teeth. The white triangles designate the locations where measurements were made at three fixed frequencies and variable thicknesses. The results for the healthy sample at selected frequencies among the frequency scan data are plotted in Figs. 4(c) to 4(e). Regardless of frequency and excitation wavelength, and consistent with thermal infrared emissions from depths much greater than the frequency-dependent thermal diffusion length, it was observed that the PTR amplitudes exhibited significant variations for thicknesses in the 10- to 7-mm range and then decreased slightly with decreasing thickness down to around 2.5 to 3 mm, rising to a peak at about 1.5 mm, followed by a rapid decrease below 1 mm. The decreasing signal region between 7 and 3 mm is probably due to gradually increasing losses of the optical source signal through back-surface transmission.

Photothermal interference can occur as a result of direct IR photon emissions. The phase signals for 659 nm [Fig. 4(c)] showed a slight evidence of thermal-wave interference for the thinnest slices, but among the optically more penetrating 830-nm signal phases [Fig. 4(d)], only the 4.7-Hz and 31.6-Hz curves had sufficient signal-to-noise ratio to show measurable differences as a function of thickness below 5 mm. It should be noted that absolute PTR signal levels were almost twice as high under 659-nm excitation, owing to the shallower optical penetration and higher power density at that wavelength. The LUM amplitude and phase at 659 nm [Fig. 4(e)] exhibited trends similar to the PTR signal in terms of both frequency and thickness variations, albeit with smaller peaks in the amplitude curves between 1 and 1.5 mm, thus giving further support to the mechanism of transmitted power loss. The LUM phase frequency order is different from the PTR and LUM amplitude curves, reflecting the approximately millisecond relaxation time domination of that channel.[19]

In conclusion, both PTR and LUM exhibit sensitivity to healthy-tooth thickness $\leqslant 10$ mm, with most pronounced dependence in the <5-mm range (PTR, both wavelengths, all

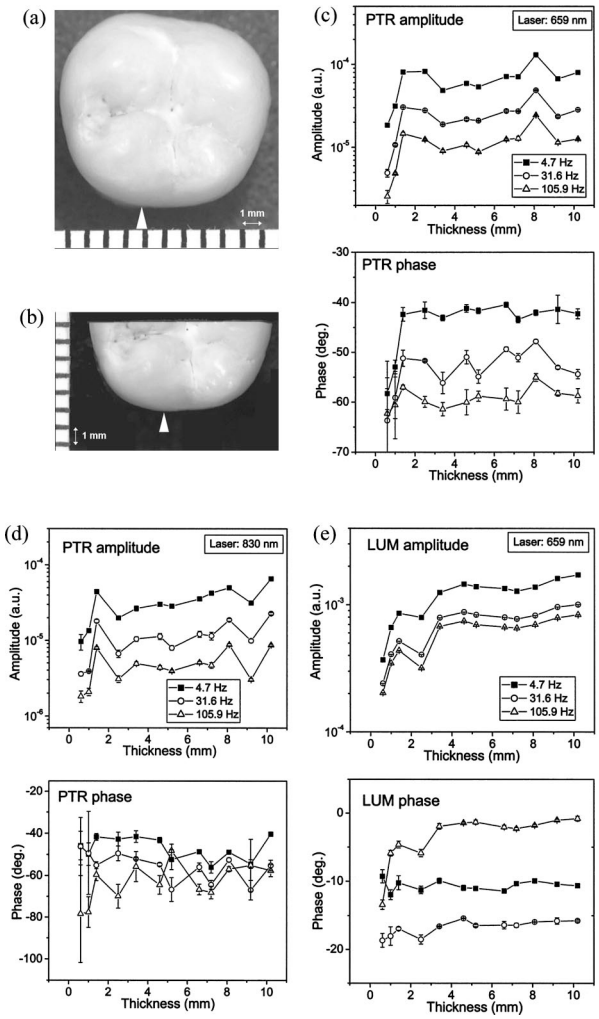

Fig. 4 Photographs and experimental results of a healthy tooth, case I-C. (a) Top view of the tooth. A white triangle designates the measurement location. (b) Same as in (a) after partially removing the opposing surface. (c) PTR amplitude and phase signals versus back-sliced sample thickness at different modulation frequencies of the 659-nm laser intensity. (d) Similar to (c) with the 830-nm laser. (e) LUM amplitude and phase signals versus back-sliced sample thickness at different frequencies with the 659-nm laser.

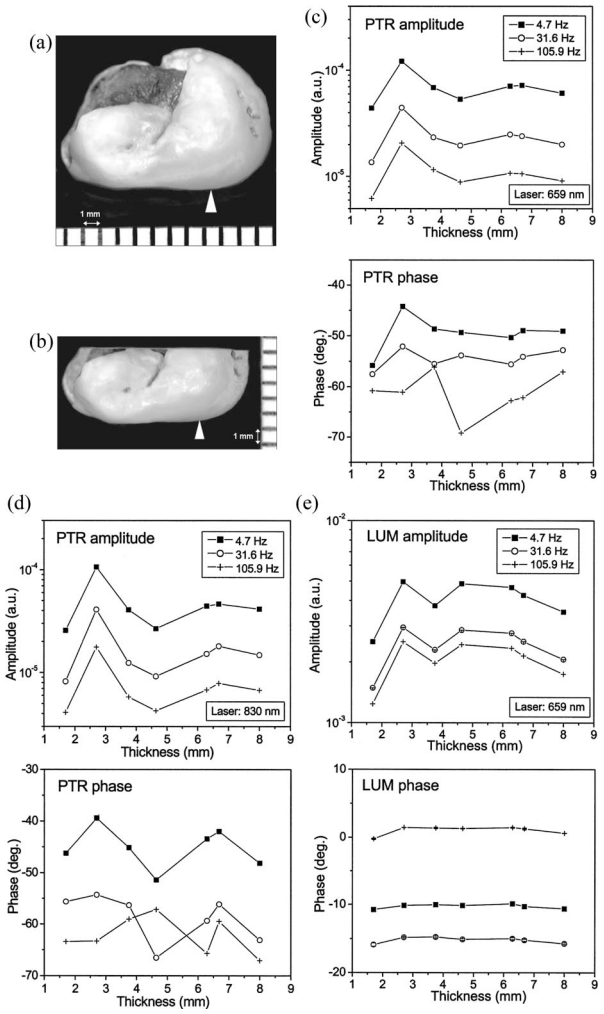

Fig. 5 Photographs and experimental results of a carious tooth, case I-C. (a) Top view of the tooth. A white triangle designates the measurement position. (b) Same as in (a) after partial grinding off of the rear surface and most of the caries. (c) PTR amplitude and phase signals versus back-sliced sample thickness at different modulation frequencies of the 659-nm laser intensity. (d) Similar to (c) with the 830-nm laser. (e) LUM amplitude and phase signals versus back-sliced sample thickness at different frequencies with the 659-nm laser.

amplitudes and phases except the 105.9-Hz phase at 830 nm owing to low-signal noise; LUM, amplitudes and 31.6 Hz, 105.9-Hz phases only). Further work is needed to quantify the observed features in terms of photothermal and luminescence interferometry. The error bars shown in Figs. 4(c), 4(d), and 4(e) are typical of the error between measurements.

The second (carious) sample of this case [Figs. 5(a) and 5(b)] exhibited peaks at all three frequencies of the 659-nm PTR signal amplitude curves [Fig. 5(c)]; however, all features were sharper than those of Fig. 4(c). The amplitude peaks appear to be shifted to ~2.7 mm thickness compared with the ~1.6 mm peaks of the healthy-tooth amplitudes of Fig. 4(c), although it should be noted that the precision of determining peak position is rather poor because of the large sampling distance (ca. 1 mm) between data points. The photothermal interferometric trough[28] behind the peak is also more pronounced in all amplitudes of Fig. 5(c) and in the 4.7-Hz and 31.6-Hz phases. The 105.9-Hz phase is somewhat compromised by a low signal-to-noise ratio. The interferometric effects become even stronger under 830-nm radiation [Fig. 5(d)].

These photothermal interferometric effects in both Figs. 5(c) and 5(d) support the interpretation that the presence of the carious region within 5 mm of the probed surface disrupts the optical and thermal homogeneity of the dental tissue and creates a remote secondary photothermal-wave source of PTR signal in the healthy region in front and to the side of the caries [note probe location in Figs. 5(a) and 5(b)]. This is due to enhanced optical absorption and thermal localization within the dark carious region with a higher absorption coefficient and poorer thermophysical property at the excitation (and perhaps infrared emission) wavelengths. In addition, deeper changes in the properties of the tooth may have occurred as demineralization in front of the advancing caries. These co-

operative effects result in larger amplitude increases and up to 10 deg higher phase lags compared with healthy teeth, which are quite sensitive to thicknesses up to 8 mm. The similarities of the curves for interference versus thickness in Figs. 5(c) and 5(d) at different frequencies indicate that the IR signals generated by the thermal waves are mostly due to direct IR emissions (radiation heat transfer), rather than originating in conductive transfer to the tooth surface. Only within the uppermost 1 mm do conductive thermal waves contribute to the signal, thus affecting the phase shapes within one thermal diffusion length from the surface [Figs. 5(c) and 5(d)].

The LUM signals [Fig. 5(e)] also exhibited higher overall amplitudes than their healthy counterparts, which is consistent with reported dc luminescence measurements at similar wavelengths.[8,9] The peak feature around 2.7 mm is consistent with the PTR signals and appears with the same frequency order, as shown in Fig. 5(e). The trough at ca. 4.5 mm (PTR signals) is juxtaposed with a LUM peak at the same thickness, further corroborating the different origins of signal interference mechanisms (photothermal versus optical) of these two signal channels. The LUM amplitude in Fig. 5(e) shows that this channel remains relatively high as long as there is a physical presence of the subsurface lesion at ca. 4 mm below the probed surface [Fig. 5(a)]. The LUM phase remains relatively insensitive to thickness variations. Once the carious material is filed away, the LUM amplitude decreases (3.4-mm thickness) and it increases again for smaller thicknesses owing to backpropagating luminescence interference contributions from the back tooth/air interface (see also case III).

With artificially thinned teeth, given the losses of transmitted laser power, of luminescence, and of thermally generated infrared photons (reflected, absorbed, and converted), the signal decreases observed at thicknesses below 1 mm are expected. Bulk phenomena such as direct optical absorption and thermal-wave generation in the carious region and optical interferences and scattered laser light or luminescence confinement in the presence of interfaces with subsurface lesions, render PTR and LUM signals sensitive to the lesion under modulated detection, despite the turbidity of dental tissue. Therefore, as a result of interface-mediated confinement, which affects optical and thermal fluxes, both the PTR and the LUM signals are maximized at around 1.4-mm thickness in healthy teeth, whereas shifts of the maximum to thicker samples occur in the presence of equivalent subsurface lesions from secondary sources [$\sim$2.7 mm in the case of Fig. 5(a)] because the highly absorbing lesion strongly confines the extent of optical penetration and enhances thermal conversion. In conclusion, direct infrared radiation thermal-wave emission and luminescence interferometry appear to be the major depth-profilometric mechanisms of PTR and LUM in teeth with subsurface carious lesions.

3.1.4 *Edge effects on subsurface feature resolution*

Figure 6(a) shows an angled view of a sectioned tooth with an approximately 1-mm diameter hole drilled near the outer surface at a minimum depth of 1 mm (case I-D). In order to study the influence of the horizontal surface on the PTR and LUM signals, two spatial scans were performed at distances 1 and 0.5 mm away from the horizontal edge of the cross-sectioned tooth with a 659-nm laser at 5 Hz. The positions and directions of the line scans are indicated by arrows in Fig. 6(a). In

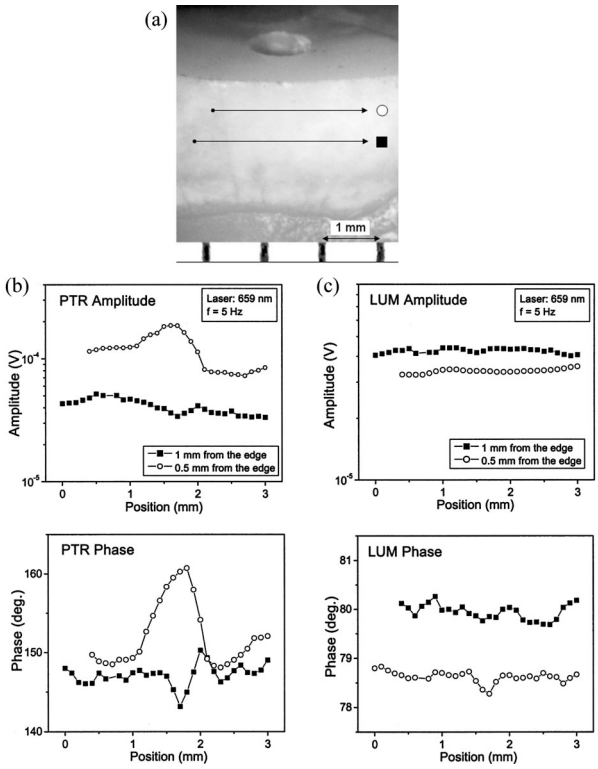

Fig. 6 Photograph and experimental results of the sample tooth, case I-D. (a) An angled view of the sectioned tooth showing a drilled hole and scan lines at two distances from the enamel edge. (b) PTR and (c) LUM amplitude and phase signals across the two scan lines at 5 Hz with the 659-nm laser.

Fig. 6(b) the PTR amplitude and phase exhibit a better overall sensitivity to the presence of the hole than the LUM scans.

It is interesting to note that the spatial confinement of the thermal-wave, radiative and conductive, by the air-to-tooth boundary at the large horizontal interface (upper ground surface) increases the PTR overall signal (0.5-mm scan) and thus enhances the resolution of the hole, while the opposite is true about the LUM amplitude because a larger fraction of the emitted luminescence escapes out of the flat upper surface in the case of the 0.5-mm scan from the edge. The PTR signal enhancement is consistent with general trends in photothermal-wave theory at edges and wedges.[28] The LUM scan exhibits much poorer resolution of the subsurface hole [Fig. 6(c)], especially the amplitude scan. The LUM phase scan shows some correlation with the PTR phase in the position of the hole (between 1 and 2 mm), especially the 0.5-mm scan away from the upper surface. In conclusion, thermal-wave confinement effects near hard tissue enamel edges tend to enhance the resolution of subsurface features, whereas the opposite happens with the LUM amplitude, resulting in a decrease and no clear trend with regard to resolution.

3.2 *Case II. Detection of Natural Lesions*

Several teeth with carious lesions, including a demineralized carious fissure at the dentin and a tooth with a crack in the enamel were examined with the PTR and LUM probes. The following three examples were part of a larger set of teeth we examined with these probes.

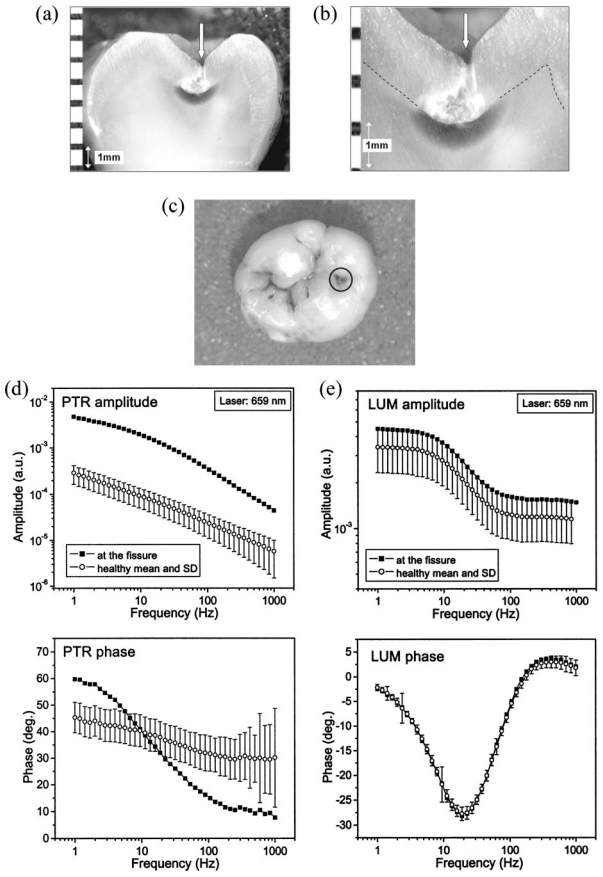

Fig. 7 Photographs and experimental results of a sample tooth in case II-A. (a) Vertical cross-section through the occlusal fissure with the measurement point indicated by a white arrow. (b) A magnified view of (a) showing the extent of subsurface demineralization (the dense white region around the fissure). The dashed lines indicate the DEJ. (c) Biting or occlusal surface of the tooth with the measurement area spot circled. (d) PTR and (e) LUM amplitude and phase frequency scans at the fissure compared with the healthy mean value and population-weighted standard deviation.

3.2.1 *Carious occlusal fissure*

Frequency scans from 1 Hz to 1 kHz were performed on suspicious occlusal fissures with the 659-nm laser source, and PTR and LUM signals were compared with signal statistics[30] obtained from healthy, smooth occlusal, buccal, or lingual surfaces (52 teeth and 332 measurement points (176 fissures, 156 smooth surfaces; case II-A)). Then the teeth were sectioned for histology using reflected light microscopy. Figures 7(a) and 7(b) show the cross-section of one of the occlusal fissures. It is clear that the demineralization is quite advanced, spreading out away from the fissure wall into the enamel, the DEJ, and the dentin. In contrast, visual inspection of the outer edges of the fissure before sectioning, shown in Fig. 7(c), could not reveal the extent of the demineralization and carious lesion.

Figure 7(d) shows PTR amplitude and phase frequency scans obtained with the laser incident directly on the fissure surface. These curves are compared with the mean and the population-weighted standard deviation[30] of scan results obtained from the healthy sample statistics. It is clear that the PTR signal indicates a strong deviation from the healthy signal norm. The amplitude [Fig. 7(d)] is more than one order of magnitude higher than the healthy mean and exhibits a pronounced curvature around 10 to 20 Hz, instead of the nearly straight-line behavior of the healthy mean-value curve. The PTR phase in Fig. 7(d) also shows features that are remarkably dissimilar to the healthy mean value, both in total phase shift over the frequency range of the scan as well as in the much steeper slope in the range coinciding with the pronounced amplitude curvature.

These dissimilarities are expected from the depth profilometric character of PTR since the geometry and thermal properties of the region that produces the signal determine its frequency dependence. For this reason and for reasons having to do with the large variations in the degree of inhomogeneity in the morphologies of carious lesions from tooth to tooth, the irregular and distorted PTR and LUM signals from such lesions cannot be grouped together as easily as can be done with the much more uniform signals from healthy enamel, to produce a statistically meaningful ''mean value'' and ''standard deviation.'' For optimal diagnostic efficiency, it was found that each case must be separately compared with the healthy reference signal bands as shown in Figs. 7(d) to 7(e).

The increased amplitude of the carious section is due to the degraded thermal properties of the heavily demineralized region below the surface [Figs. 7(a) and 7(b)]. The poorer thermal properties are accompanied by higher optical absorption properties at and below the surface, resulting in an increased thermal-wave field and stronger infrared PTR emissions. The large low-frequency PTR phase lag is indicative of the stronger absorption and thermal emission from the demineralized region. This subsurface thermal-wave source (radiative in nature) shifts the thermal-wave centroid deeper into the enamel, close to the dentin-enamel junction, thus advancing the low-f phase lag with respect to the healthy mean.

At high frequencies, the importance of the subsurface demineralized region diminishes because the thermal-diffusion length shrinks and the major PTR signal contribution (mostly conductive in nature) originates close to the surface the site of the visibly dark spot (circled) of Fig. 7(c). As a result, the thermal-wave centroid moves very close to the surface, exhibiting a smaller phase lag than the healthy mean. This is accompanied by a steep amplitude gradient with the changeover of the thermal-wave source to one lying on the surface. The phase-dominating thermal-wave centroid shift controls the steep phase gradient in the intermediate frequency range. Therefore, the steep slope is characteristic of carious subsurface lesions acting as thermal-wave sources, even though absolute phase values may lie within the healthy range.

On the contrary, the LUM amplitude and phase shapes are statistically indistinguishable from that of the healthy means. The amplitude curve lies within the population-weighted standard deviation, albeit at the upper end of the range (it should be noted that carious regions are associated with increased luminescence emissions at this wavelength[8,9]). From this viewpoint, the LUM amplitude corroborates the PTR trends, in that although it is located near the upper limit of the standard deviation of the healthy mean, the LUM amplitude is at the boundary of the healthy mean at all frequencies, indicating a suspicious fissure. The LUM phase was found to be quite insensitive to the presence of the caries or demineralization and lies entirely within the healthy range [Fig. 7(e)]. These

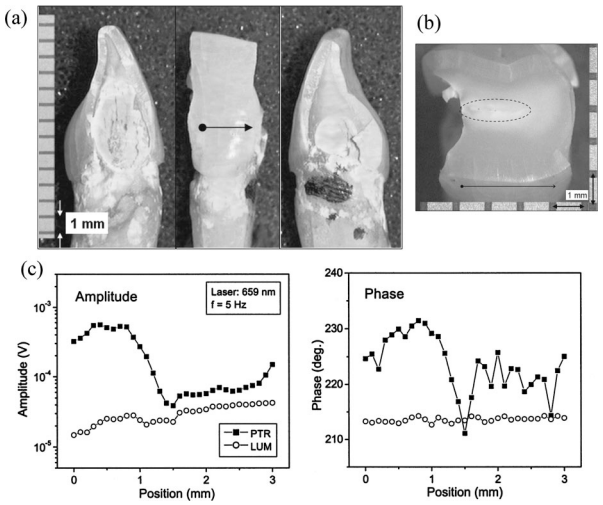

Fig. 8 Photographs and experimental results of the sample tooth in case II-B. (a) Left, front, and right views of a mandibular incisor. (b) Cross-section at the scan line at the level of the arrow in (a), highlighting a deep demineralized lesion (dotted region in the middle). (c) PTR and LUM amplitude and phase signals across the scan line at 5 Hz and 659 nm.

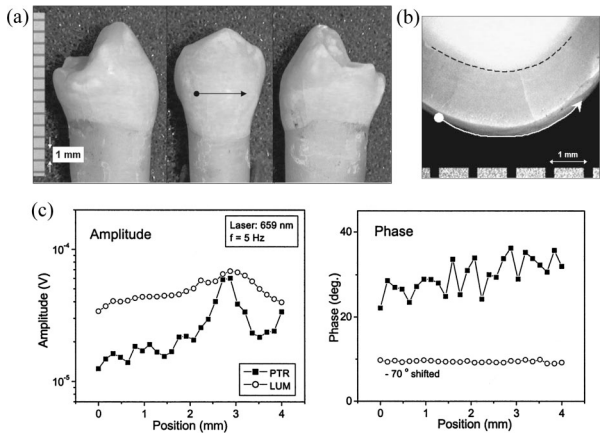

Fig. 9 Photographs and experimental results of a mandibular bicuspid with a radial enamel crack in case II-C. (a) Left, front, and right views of the tooth. (b) Cross-section at the scan level showing the radial crack. The DEJ is highlighted to aid the eye. (c) PTR and LUM amplitude and phase signals across the scan line at 5 Hz.

results clearly show the sensitivity of depth profilometric PTR to the presence of advanced demineralization and caries within an occlusal fissure and the usefulness of the LUM probe in corroborating the PTR phase, albeit with diminished sensitivity.

3.2.2 *Deep subsurface carious lesion in dentin*

The horizontal cross-section of a mandibular central incisor with a large carious lesion on both interproximal surfaces is shown in Fig. 8(a). Figure 8(b) is a view of the horizontal cross-section at a level indicated by the arrow in Fig. 8(a). It shows (highlighted) the carious lesion involving most of the dentin, and a section of the pulp horn just beneath the dentin surface (case II-B). The white area within the highlighted region is actually dentin that is not highly mineralized since it is very near the pulp and contains a large number of tubules, much higher than dentin near the DEJ. The arrow in Fig. 8(b) shows the direction and extent of the laser scan across the intact side surface of the tooth corresponding to the arrow in Fig. 8(a). The spatial scan results with the 659-nm laser as a source modulated at 5 Hz are shown in Fig. 8(c). From the onset to the middle of the scan, the PTR amplitude is high (5×10^{-4} V range) over the region, which is consistent with the presence of the deep subsurface lesion at approximately 2.5 mm below the tooth surface. The PTR signal drops to ca. 5×10^{-5} V outside the carious region and rises slightly again close to the right edge of the tooth (a thermal-wave edge effect[28]).

The LUM amplitude also shows a similar structure but far less dramatic contrast than the PTR amplitude, a further indication of the nondepth profilometric nature of modulated luminescence since signal strength is weighed equally from all subsurface depths. This LUM response is consistent with the hypothesis that the depth sensitivity of luminescence is mainly due to the presence of interfacial phenomena and is highest when abrupt optical interfaces are involved (Fig. 3 and Fig. 4), unlike the case of Fig. 8(b), which shows a gradual change in the optical (scattering) properties of the dentin in the neighborhood of the subsurface lesion. The difference in sensitivity to the deep subsurface lesion between PTR and LUM is consistent with case I-B (Fig. 3); that is, PTR is more sensitive to deeper inhomogeneities than LUM, even when sharp boundaries are involved. In a manner similar to the phase behavior of a carious region with gradually changing properties [Fig. 8(c)], the sharp-boundary PTR phase [Fig. 3(c)] exhibits strong spatial dependence correlated to the PTR amplitude, while the LUM phase shows little correlated variation. The low-frequency (<100 Hz) insensitivity of the LUM phase [Fig. 8(c)] to subsurface dental structure has been noted earlier.[19]

3.2.3 *Enamel cracks*

The tooth shown in Fig. 9(a) is healthy, but there is a natural radial crack in the thick enamel, as shown on the top-down cross-sectional plane of Fig. 9(b) (case II-C). The spatial scan results along the white arrow with the 659-nm laser at 5 Hz are shown in Fig. 9(c). Dashes have been added at the enamel/dentin junction to aid the eye. A sharp PTR amplitude peak and a shallow, broadened, LUM amplitude peak caused by the crack are shown around 2.8 mm from the scan onset coordinate point. PTR shows higher spatial resolution and contrast than LUM because the latter is more sensitive to scattered excitation light at the crack, which broadens the region from which multiscattered luminescence photons are collected. The PTR signal is primarily due to the thermal discontinuity in the cracked region, which occurs along the actual crack configuration and is thus more representative of the actual extent of the crack. The fact that there are no significant changes in the PTR phase scan indicates that thermal-wave flux disruption occurs mainly sideways as the laser beam sweeps across the walls of the crack, rather than impeded flux along the depth coordinate, a phenomenon well known from mirage-effect measurements in the nondestructive evaluation of cracks in engineering materials.[21,23]

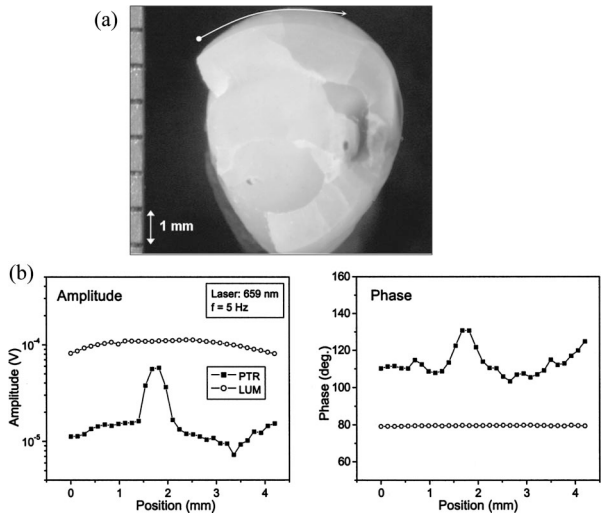

Fig. 10 Cross-sectional photograph and experimental results of a sample tooth with a slanted enamel crack in case II-C. (a) Cross-section at the scan level showing the slanted crack. The dark region at the end of the scan is carious. This area was not scanned. (b) PTR and LUM amplitude and phase across the scan line at 5 Hz with the 659-nm laser.

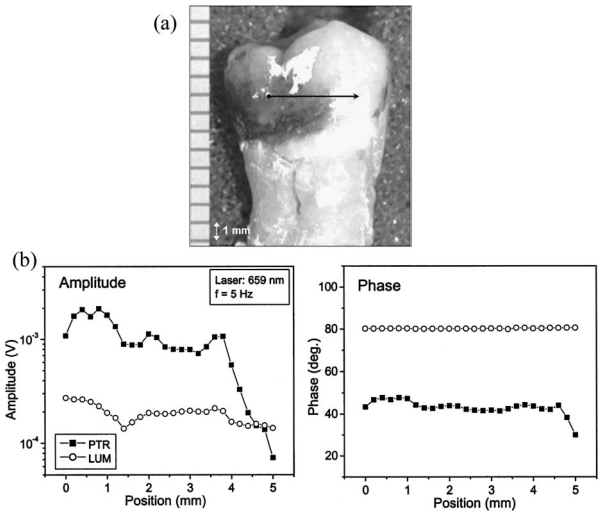

Fig. 11 Photograph and experimental line-scan results of a maxillary molar with a surface stain in case II-D. (a) View of the stained region and scan location. (b) PTR and LUM amplitude and phase across the scan line at 5 Hz using the 659-nm laser source.

Unfortunately, the expected small phase variation from the lateral thermal impedance represented by the crack wall is lost in the noise of Fig. 9(c) because the overall healthy tooth generates low PTR signals less than 10^{-4} V. It has been found that as a rule, healthy and thick enamel generates small PTR and LUM amplitudes (<0.1 mV). The LUM phase shows no contrast, which is consistent with the insensitivity of this signal channel to dental irregularities at low frequencies.

Another similar healthy tooth sample with a slanted natural crack is shown in Fig. 10(a). The deep crack in the enamel layer in the middle of the scan line is clearly visible. Both PTR amplitude and phase show sharp peaks at this location, whereas the LUM amplitude and phase exhibit no contrast at all. The phase sensitivity to the crack is due to the slanted nature of the crack, which may impede heat flux in the radial depth direction as well as in the tangential direction, thus amounting to a considerably larger effective thermal impedance than the crack of Fig. 9(b).

In summary, successful PTR detection of natural subsurface cracks in teeth, also reported earlier,[19] depends on the size, orientation, and depth of the crack. LUM detection is unpredictable and may possibly distort the geometric shape of the crack.

3.2.4 *Surface stain*

Figure 11(a) shows a left maxillary first molar with a large dark stain on the left side (case II-D). The scan line and direction indicated by an arrow start inside the stain and end at a relatively healthy-looking region. Figure 11(b) shows the experimental results with the 659-nm laser at 5 Hz. The PTR amplitude is very high ($>10^{-3}$ V) within the stained region, as expected from the high optical absorption coefficient of the stain, and exhibits some structure. The PTR phase shows little contrast across the stain border, indicating that the dark region is mostly a surface feature. It is well known that surface absorptions affect the thermal-wave amplitude but not the phase, which is the ratio of the lock-in amplifier quadrature and in-phase signals and is thus independent of the surface reflectivity of the sample.[23] Therefore, Fig. 11(b) shows that a combination of amplitude and phase scans in PTR dental surface diagnostics can be used successfully to distinguish surface stains from other dark-colored carious features that may extend below the surface region. The latter can change the low-frequency phase significantly when the extent of the carious feature is on the order of the thermal diffusion length $\mu(\omega)$ in the enamel. Unfortunately, this important criterion cannot be applied to LUM signals because the LUM phase is always flat at low frequencies. Nevertheless, the LUM amplitude across the stain shows some correlation with the PTR amplitude, but the latter exhibits much higher spatial resolution.

3.2.5 *Extended carious cavity on the far side of a tooth*

Spatial scans were performed on the visually healthy surface of a mandibular bicuspid [Fig. 12(a)], which, however, hides a large carious cavity on the opposite side, 3- to 5-mm deep, as revealed in the top-down cross-sectional picture [Fig. 12(b)] (case II-E). As shown in the scans of Figs. 12(c) and 12(d), performed along the arrow in Figs. 12(a) and 12(b), the PTR amplitude and phase measured with the two lasers at two frequencies, 5 and 30 Hz, vary drastically across the carious region. Especially noticeable are the two peaks in the 1.5- to 3-mm range, which are exhibited by both amplitude and phase and can be directly associated with the irregular white (light-scattering) demineralized features surrounding the dark carious pulp tissue at the center of the scan. The amplitude resolution of these two peaks is highest for the deeper-penetrating 830-nm radiation at the smaller thermal wavelength of 30 Hz [Fig. 12(d)]. The 30-Hz PTR phase, however, exhibits lower peak resolution than the 5-Hz phase, indicating the deep origin of these features, which are beyond the reach of the 30-Hz PTR thermal-wave probe.

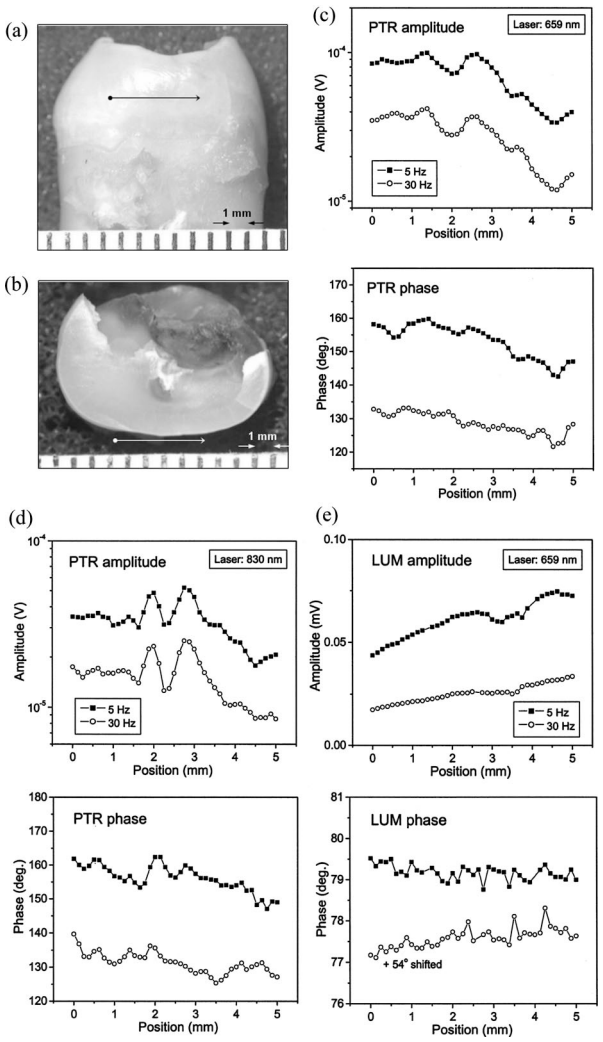

Fig. 12 Photographs and line-scan results of the sample tooth with deep subsurface caries in case II-E. (a) Front surface of the tooth with the scan line indicated (black arrow). (b) Top view of the cross-section at the level of the scan line (white arrow). (c) PTR amplitude and phase across the scan line at 5 Hz and 30 Hz with the 659-nm laser. (d) Similar to (c) with the 830-nm laser. (e) LUM amplitude and phase across the scan line at 5 and 30 Hz with the 659-nm laser.

The decreasing PTR amplitude and phase lag to the right of the peaks is probably due to the excessive thinning out of the sound dentin and the concomitant loss of source power to the backing (air), which tends to eliminate contributions of infrared emissions from that region and shift the thermal-wave centroid (phase) closer to the front surface. These trends are similar to those observed with the artificially drilled holes in Fig. 3. The PTR signal increase beyond 4.5 mm may also be due to the onset of thermal-wave interference within the critically thinned enamel-dentin region. The LUM amplitudes in Fig. 12(e) show little structure, mostly in the region of the second peak at 5 Hz, a broadened feature believed to be due to backpropagation of scattered luminescence photons from the thinned carious interface. The LUM phase is noisy and entirely structureless.

In summary, PTR scanning can be used to identify deep subsurface carious regions with various degrees of demineralization. The deeply penetrating 830-nm laser source range and relatively high modulation frequency are best suited for optimal amplitude spatial resolution of the carious features, while the low-frequency PTR phase resolves subsurface carious features best. LUM detection appears to be less capable of monitoring these deep lesions.

3.3 *Case III. Determination of DEJ Depth*

Two healthy teeth were chosen to study how the PTR and LUM signals depended on naturally varying enamel thickness and on distance from the DEJ along the proximal surface of a tooth. One tooth was probed with both lasers in our system. The thickness of the enamel at each side surface examined ranged between 0 and 1.26 mm for the first sample [Fig. 13(a)] and 0 to 1.69 mm for the second sample [Fig. 14(a)]. In Fig. 13(a) and Fig. 14(a), dashes have been added along the DEJ to aid the eye. As shown in Figs. 13(b) to 13(e) and Figs. 14(b) and 14(c), the PTR amplitude decreases as the thickness of the enamel increases, until the scan reaches a certain point away from the DEJ at the surface [1.03 mm for Figs. 13(a) and 13(c) and 0.99 mm for Figs. 14(a) and 14(c)], where the PTR amplitude starts increasing. This nonmonotonic increase [Figs. 13(c) and 13(e) and 14(c)] is most likely due to the high curvature of the scanned enamel surface at positions 6 and 8 in Fig. 13(a) and Fig. 14(a), respectively. Highly curved surfaces resemble edges photothermally, which tends to confine thermal-wave power, thus increasing photothermal signals.[28]

The PTR phase curves in Figs. 13(b) and 13(d) show only slight differences and only at low and high frequency ranges; however those in Fig. 14(b) show considerably larger differences. Similarly, the PTR amplitudes in Figs. 14(b) and 14(c) exhibit greater variation with distance from the DEJ than Figs. 13(b) and 13(c). These differences seem to be caused by the strongly inhomogeneous (demineralized) dark and white regions inside the dentin below the DEJ in Fig. 14(a).

Overall, larger PTR signals at shallower enamel thicknesses are consistent with thermal-wave confinement above the DEJ, with a concomitant increase in the thermal energy content of the region owing to the poorer thermophysical properties (diffusivity, conductivity) of dentin.[27] The ability of PTR signals to penetrate through the DEJ and monitor inhomogeneities deep in the dentin is an important manifestation of the depth profilometric potential of this technique past natural dental interfaces. The LUM signal in Fig. 13(g) for the first (sub-DEJ homogeneous) sample shows trends similar to the PTR signal (increasing amplitude with decreasing thickness), as expected from an enhanced luminescence intensity field under interfacial confinement within the enamel region, where signal contributions from reflections and backpropagation from the interface increase with decreasing thickness of the enamel. For less than 0.3 mm of enamel, however, much optical power is lost to the dentin and subdentin region, with the result that LUM amplitudes start to decrease [Fig. 13(g) and Fig. 14(e)] in a manner consistent with the results of the artificially thinned enamel of Fig. 4. While LUM phases are essentially flat for the homogeneous tooth of Fig. 13(g), they exhibit stronger variations in Fig. 14(e), thus corroborating the much larger variations of the PTR phases [Fig. 14(c)].

In summary, thermal-wave confinement within naturally occurring dental layers, such as in the case of variable-depth DEJs, in the proximal surfaces, can be useful in measuring the

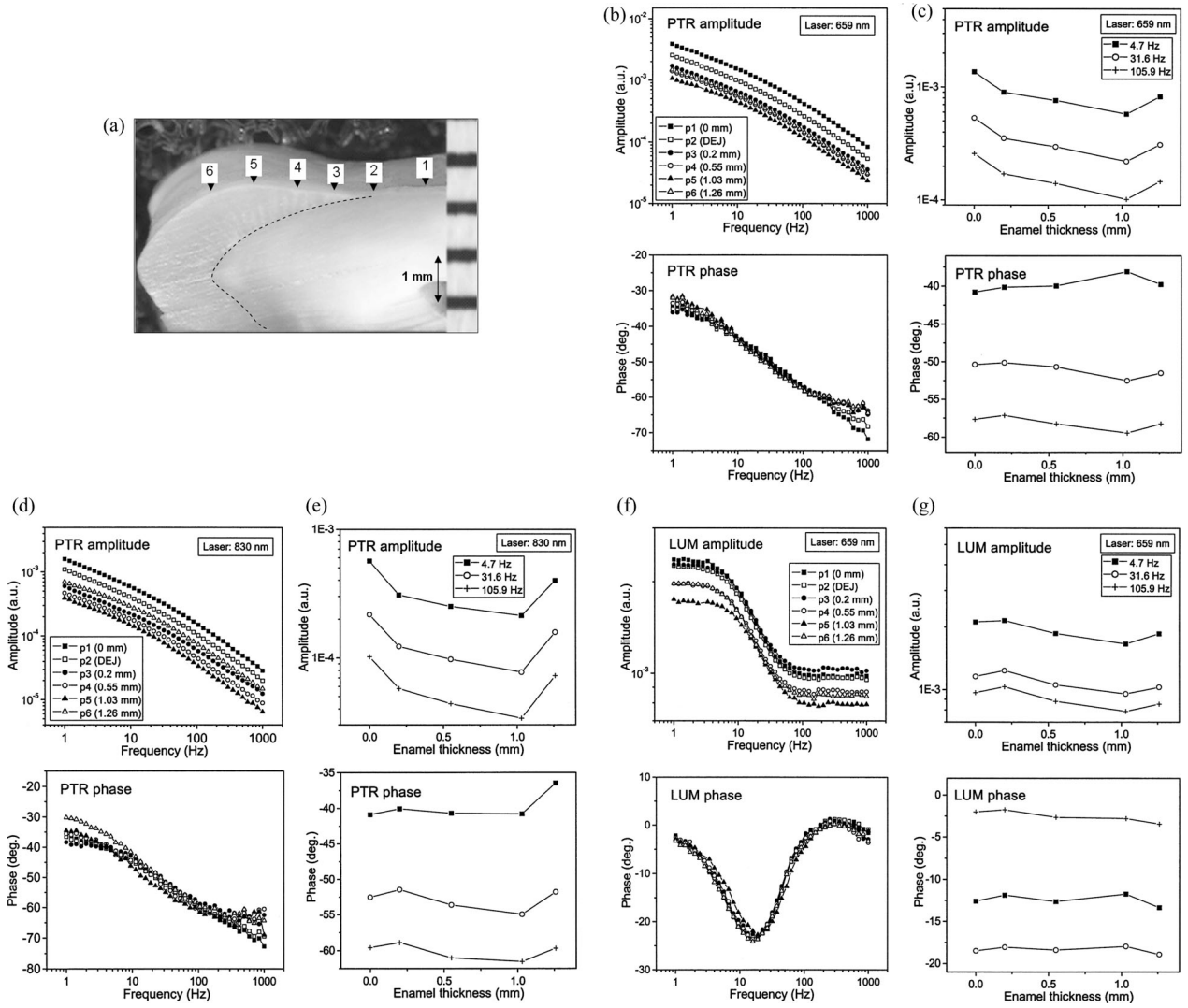

Fig. 13 Cross-sectional photograph and experimental results of a tooth with a variable enamel thickness and healthy enamel and dentin in case III. (a) Side view of the cross-section of the tooth with the measurement points indicated, and a dashed line outlining the DEJ to aid the eye. (b) PTR amplitude and phase frequency scans at the points indicated in (a) with different enamel thicknesses; 659-nm laser. (c) PTR amplitude and phase signals versus enamel thickness at selected frequencies from (b). (d) Same as in (b) with 830-nm laser. (e) PTR amplitude and phase signals versus enamel thickness at selected frequencies from (d). (f) LUM amplitude and phase signals of frequency scans at the points indicated in (a) with different enamel thicknesses; 659-nm laser. (g) LUM amplitude and phase signals versus enamel thickness at selected frequencies from (f).

distance of the DEJ by means of PTR frequency scans at spots away from high-curvature surfaces. There is evidence that sub-DEJ material inhomogeneities (demineralization) can also be monitored from the scatter they cause to the PTR phase frequency scans along the proximal surface [Fig. 14(b)]. LUM amplitude variations with DEJ depth have also been observed; however, they are nonmonotonic, even far from high-curvature locations. Therefore it is not clear whether they can be used for estimating that depth.

4 Conclusions

Using simultaneous nonintrusive, noncontacting PTR and LUM imaging techniques, several case studies of depth profilometric diagnosis in human teeth have been described, including (case I) detection of artificial subsurface holes and variations in tooth thickness variations; (case II) detection of natural carious lesions; and (case III) determination of DEJ depth. These investigations have been performed with two near-IR source wavelengths (659 and 830 nm) from semiconductor lasers. The major findings for each case are as follows. PTR and LUM are able to detect artificial subsurface defects with sharp boundaries at depths greater than 5 mm, with PTR exhibiting superior sensitivity and contrast to both the presence of, and changes in, the sharp boundaries, as well as to changes in natural carious inhomogeneities (demineralized regions) of the tooth.

PTR line-scan imaging has depth profilometric capabilities, monitoring artificial defects at least up to 3 mm below the surface. This feature should allow clinicians to detect carious lesions on both the occlusal surface (biting or top surface of the tooth) and the interproximal or contact area of the tooth (an area that has traditionally required using dental X-rays).

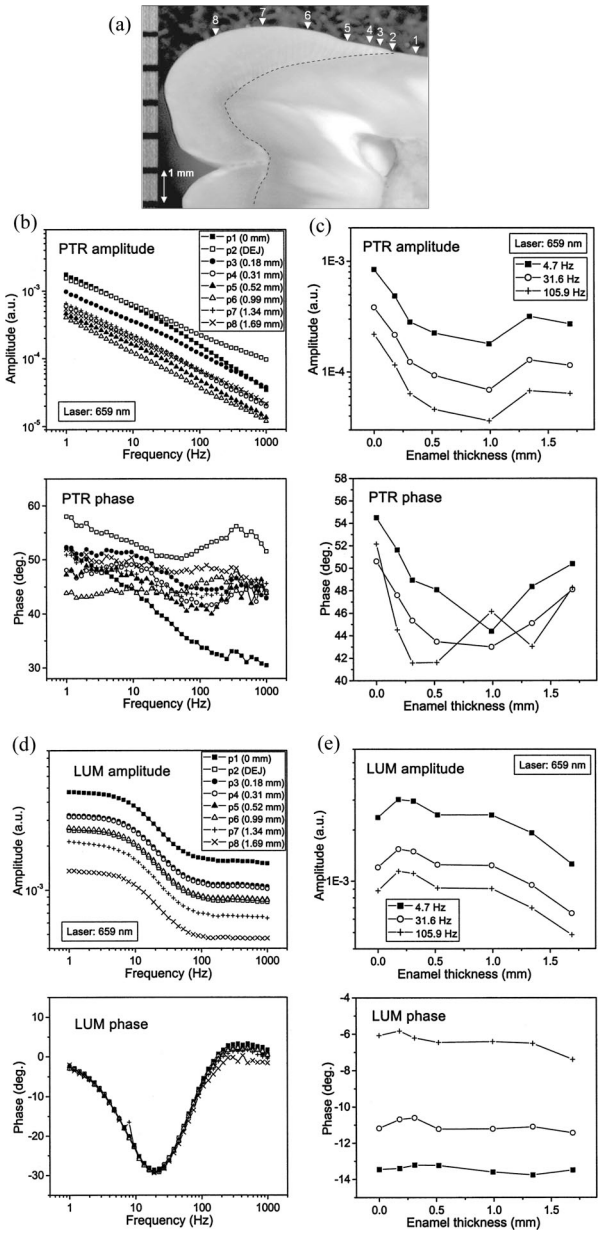

Fig. 14 Cross-sectional photograph and experimental results of a tooth with variable DEJ distance and inhomogeneous dentin in case III. (a) Side view of the cross-section of the tooth with the measurement points indicated, and a dashed line outlining the DEJ to aid the eye. (b) PTR amplitude and phase frequency scans at the points indicated in (a) with different enamel thicknesses; 659-nm laser. (c) PTR amplitude and phase signals versus enamel thickness at selected frequencies from (b). (d) LUM amplitude and phase signals of frequency scans at the points indicated in (a) with different enamel thicknesses; 659-nm laser. (e) LUM amplitude and phase signals versus enamel thickness at selected frequencies from (d).

However, LUM scans appear to exhibit much lower resolution and contrast than PTR to localized, artificially made, subsurface defects in teeth. Direct thermal infrared radiation emission and luminescence interferometry appear to be the major depth profilometric mechanisms of PTR and LUM in teeth with subsurface carious lesions. LUM depth-sensitive signal mechanisms are consistent with equally weighted contributions from all probed depths, unlike the modulation-frequency-controlled depth information content of the PTR signal. Thermal-wave confinement effects near hard enamel edges tend to enhance the resolution of subsurface features, whereas a decrease in LUM amplitude results in no clear trend with regard to resolution. The sensitivity of depth profilometric PTR to the presence of advanced demineralization within an occlusal fissure and the usefulness of the LUM probe in corroborating the PTR phase, albeit with diminished sensitivity, was demonstrated. PTR detection of natural subsurface cracks in teeth depends on the size, orientation, and depth of the crack, while LUM detection is unpredictable and may possibly distort the geometric shape of the crack.

Regarding the diagnosis of caries, the deeply penetrating 830-nm laser source range and relatively high modulation frequencies are best suited for optimal-amplitude spatial resolution of subsurface carious features, while the low-frequency PTR phase better resolves these carious features. LUM detection appears to be less capable of monitoring deep lesions. More work will be required to sort out signal dependence on the type, size, and severity of subsurface carious lesions. Thermal-wave confinement within naturally occurring dental layers, such as in the case of variable DEJ depth in the proximal surfaces, can be useful in measuring enamel thickness by means of PTR frequency scans at a fixed spot away from high-curvature surfaces.

We found evidence that demineralization or changes in mineral content in the dentin can also be monitored from the scatter caused to the PTR phase frequency scans along the proximal surface. LUM amplitude variations with DEJ depth are nonmonotonic and thus it is not clear whether they can be used for estimating that depth.

In summary, it is concluded that PTR (alone or in combination with LUM) can be used as a sensitive, nonintrusive, depth profilometric dental probe for the diagnosis of near-surface or deep subsurface carious lesions and/or for monitoring the thickness of enamel.

Acknowledgments

The support of Materials and Manufacturing Ontario (MMO) with an Enabling Contract is gratefully acknowledged. The assistance of Calvin Han with some of the measurements is also acknowledged.

References

1. D. McComb and L. E. Tam, "Diagnosis of occlusal caries: Part I. Conventional methods," *J. Can. Dent. Assoc.* **67**, 454–457 (2001).
2. D. Ricketts, E. Kidd, K. Weerheijm, and H. de Soet, "Hidden caries: What is it? Does it exist? Does it matter?" *Int. Dent. J.* **47**, 259–265 (1997).
3. L. J. Brown and P. A. Swango, "Trends in caries experience in US employed adults from 1971–74 to 1985: Cross-sectional comparisons," *Adv. Dent. Res.* **7**(1), 52–60 (1993).
4. B. E. Angmar-Månsson, S. Al-Khateeb, and S. Tranæus, "Caries diagnosis," *J. Dent. Educ.* **62**, 10, 771–780 (1998).
5. H. Eggertsson, M. Analoui, M. H. van der Veen, C. González-Cabezas, G. J. Eckert, and G. K. Stookey, "Detection of early interproximal caries in vitro using laser fluorescence, dye-enhanced laser fluorescence and direct visual examination," *Caries Res.* **33**, 227–233 (1999).
6. M. D. Lagerweij, M. H. van der Veen, M. Ando, L. Lukantsova, and G. K. Stookey, "The validity and repeatability of three light-induced fluorescence systems: An in vitro study," *Caries Res.* **33**, 220–226 (1999).

7. E. H. Verdonschot, B. Angmar-Månsson, J. J. ten Bosch, C. H. Deery, M. C. D. N. J. M. Huysmans, N. B. Pitts, and E. Waller, "Developments in caries diagnosis and their relationship to treatment decisions and quality of care," *Caries Res*. **33**, 32–40 (1999).
8. R. Hibst and K. Konig, "Device for detecting dental caries," U.S. Pat. 5,306,144 (1994).
9. R. Hibst, R. Gall, and M. Klafke, "Device for the recognition of caries, plaque or bacterial infection on teeth," U.S. Pat. 6,024,562 (2000).
10. H. M. Alwas-Danowska, A. J. M. Plasschaert, S. Suliborski, and E. H. Verdonschot, "Reliability and validity issues of laser fluorescence measurements in occlusal caries diagnosis," *J. Dent*. **30**, 129–134 (2002).
11. A. Lussi, S. Imwinkelried, N. B. Pitts, C. Longbottom, and E. Reich, "Performance and reproducibility of a laser fluorescence system for detection of occlusal caries in vitro," *Caries Res*. **33**, 261–266 (1999).
12. X.-Q. Shi, S. Tranæus, and B. Angmar-Månsson, "Comparison of QLF and DIAGNOdent for quantification of smooth surface caries," *Caries Res*. **35**, 21–26 (2001).
13. X.-Q. Shi, U. Welander, and B. Angmar-Månsson, "Occlusal caries detection with KaVo DIAGNOdent and radiography: An in vitro comparison," *Caries Res*. **34**, 151–158 (2000).
14. V. D. Rijke and J. J. ten Bosch, "Optical quantification of caries like lesions in vitro by use of fluorescence dye," *J. Dent. Res*. **69**, 1184–1187 (1990).
15. D. Fried, W. Sefa, R. E. Glena, and J. D. B. Featherstone, "Thermal response of hard dental tissues to 9 through 11-μm CO_2-laser irradiation," *Opt. Eng*. **35**, 1976–1984 (1996).
16. D. Fried, S. R. Visuri, J. D. B. Featherstone, J. T. Walsh, W. Seka, R. E. Glena, S. M. McCormack, and H. A. Wigdor, "Infrared radiometry of dental enamel during Er:YAG and Er:YSGG laser irradiation," *J. Biomed. Opt*. **1**, 455–465 (1996).
17. S. Al-Khateeb, R. A. M. Exterkate, E. de Josselin de Jong, B. Angmar-Månsson, and J. M. ten Cate, "Light-induced fluorescence studies on dehydration of incipient enamel lesions," *Caries Res*. **36**, (2002).
18. A. Mandelis, L. Nicolaides, C. Feng, and S. H. Abrams, "Novel dental depth profilometric imaging using simultaneous frequency-domain infrared photothermal radiometry and laser luminescence," *Proc. SPIE* **3916**, 130–137 (2000).
19. L. Nicolaides, A. Mandelis, and S. H. Abrams, "Novel dental dynamic depth profilometric imaging using simultaneous frequency-domain infrared photothermal radiometry and laser luminescence," *J. Biomed. Opt*. **5**, 31–39 (2000).
20. A. Mandelis, "Review of progress in theoretical, experimental, and computational investigations in turbid tissue phantoms and human teeth using laser infrared photothermal radiometry," *Proc. SPIE* **4710**, 373–383 (2002).
21. G. Busse and H. G. Walther, "Photothermal nondestructive evaluation of materials with thermal waves," in *Principles & Perspectives of Photothermal & Photoacoustic Phenomena*, A. Mandelis, Ed., Vol. 1, pp. 205–298, Elsevier, New York (1992).
22. A. Mandelis, M. Munidasa, and A. Othonos, "Single-ended infrared photothermal radiometric measurement of quantum efficiency and metastable lifetime in solid-state laser materials: The case of ruby (Cr^{3+}:Al_2O_3)," *IEEE J. Quantum Electron*. **29**, 1498–1504 (1993).
23. M. Munidasa and A. Mandelis, "Photothermal Imaging and Microscopy," in *Principles & Perspectives of Photothermal & Photoacoustic Phenomena*, Vol. 1, pp. 299–367, Elsevier, New York (1992).
24. C. John, D. Wu, A. Salerno, G. Busse, and C. Löst, "Applying phase-sensitive modulated thermography to ground sections of a human tooth," in *Nondestructive Characteristics & Material VIII*, R. E. Green, Jr., Ed., pp. 757–762, Plenum, New York (1998).
25. L. Nicolaides, C. Feng, A. Mandelis, and S. H. Abrams, "Quantitative dental measurements by use of simultaneous frequency-domain laser infrared photothermal radiometry and luminescence," *Appl. Opt*. **41**(4), 768–777 (2002).
26. D. Fried, R. E. Glena, J. D. B. Featherstone, and W. Seka, "Nature of light scattering in dental enamel and dentin at visible and near-infrared wavelengths," *Appl. Opt*. **34**(7), 1278–1285 (1995).
27. W. S. Brown, W. A. Dewey, and H. R. Jacobs, "Thermal properties of teeth," *J. Dent. Res*. **49**(4), 752–754 (1970).
28. A. Mandelis, "Diffusion-Wave Fields: Mathematical Methods and Green Functions," pp. 284–296, Springer, New York (2001).
29. A. Mandelis and C. Feng, "Frequency-domain theory of laser infrared photothermal radiometric detection of thermal waves generated by diffuse-photon-density wave fields in turbid media," *Phys. Rev. E* **65**, 021909 (2002).
30. R. J. Jeon, C. Han, V. Sanchez, A. Mandelis, and S. H. Abrams, "Diagnosis of pit and fissure caries using photothermal radiometry and modulated luminescence," *Caries Res*. (in press; accepted March 2004).